THE CANADIAN JOURNAL OF CHEMICAL ENGINEERING

Modelling fast pyrolysis of biomass in a fluidized bed reactor

Maurizio Troiano[1,2] | Valeria Ianzito[1] | Roberto Solimene[2] |
Elvis Tinashe Ganda[1] | Piero Salatino[1,2]

[1]Dipartimento di Ingegneria Chimica, dei Materiali e della Produzione Industriale, Università degli Studi di Napoli Federico II, Naples, Italy

[2]Istituto di Scienze e Tecnologie per l'Energia e la Mobilità Sostenibili (STEMS), Consiglio Nazionale delle Ricerche, Naples, Italy

Correspondence
Piero Salatino, Dipartimento di Ingegneria Chimica, dei Materiali e della Produzione Industriale, Università degli Studi di Napoli Federico II, Naples, Italy.
Email: salatino@unina.it

Abstract

A compartmental one-dimensional model of a fluidized bed pyrolytic converter of biomass is presented. Reference conditions are those of non-catalytic fast pyrolysis of biomass in a shallow fluidized bed with external regeneration of the bed material. The fate of biomass and of the resulting char has been modelled by considering elutriation of biomass and char particles, char attrition as well as bed drain/regeneration. The course of primary and secondary pyrolitic reactions is modelled according to a semi-lumped reaction network using well-established kinetic parameters taken from the literature. A specific focus of the present study is the role of the heterogeneous volatile–char secondary reactions, whose rate has been modelled by borrowing a kinetic expression from the neighbouring area of tar adsorption/decomposition over char. The results of computations highlight the relevance of heterogeneous volatile–char secondary reactions and of the closely associated control of char loading in the bed. The sensitivity of the reactor performance to char elutriation and attrition, to proper management of bed drain/regeneration, and to control of gas phase backmixing is demonstrated. Model results provide useful guidelines for optimal design and control of fluidized bed pyrolyzers and pinpoint future research priorities.

KEYWORDS
attrition, biomass, fluidized bed, model, pyrolysis

1 | INTRODUCTION

Residual biomass is expected to play a major role in the transition to a decarbonized world by the progressive replacement of fossil resources in the production of biofuels and platform chemicals. While there are several conversion pathways available for the conversion of this renewable carbon source, fast pyrolysis offers a direct route for the production of liquid fuels and chemicals with greater feedstock flexibility and energy input efficiency compared to alternative thermochemical pathways. Fast pyrolysis is capable of converting all of the carbon in the feedstock, unlike biological processes, which can only valorize the non-recalcitrant fraction of biomass.[1,2] Moreover, fast pyrolysis fits well into extended-supply chain biomass valorization schemes,

Can J Chem Eng. 2023;101:110–120.

based on decentralized processing of raw feedstock and the generation of biogenic intermediates (biofeedstocks) at the biomass harvesting/collection sites that may eventually be upgraded in biorefineries.[3]

Bio-oil is generated by fast pyrolysis through a complex chemical network of series–parallel thermally activated reactions starting with early depolymerization of lignocellulosic biopolymers (cellulose, hemicellulose, and lignin), eventually followed by cracking and rearrangement/isomerization, polymerization, aromatization, volatilization, and condensation.[4–6] The inherent heterogeneity of biomass feedstocks and the complexity of the pyrolytic chemical pathways are responsible for the broad variety of chemical compounds in the bio-oil, including pyrolytic sugars and oligosaccharides, furans, alkylphenols, acids, ketones, and aldehydes, together with substantial amounts of water. The complex composition and poor properties (high viscosity, acidic pH, low heat value, and limited stability) of bio-oils may jeopardize their further processing and use.[7] For this reason, notwithstanding decades of extensive investigation of biomass pyrolysis, research is still very active in the attempt to improve the design of pyrolytic converters and the choice of process conditions that maximize yield and selectivity toward valuable compounds. Catalytic pyrolysis,[8–11] fractional/staged pyrolysis,[12,13] and co-pyrolysis with non-recyclable plastics,[14] represent some of the variants of basic isothermal non-catalytic fast pyrolysis that are currently being explored to accomplish this goal.

A fundamental prerequisite for improved pyrolysis yield and selectivity is clever chemical reaction engineering of the pyrolytic conversion, with the aim of ensuring thorough control of the reaction environment and conditions. The present study is focused on fluidized bed fast pyrolysis, selected due to its versatility, robustness, and superior thermal performance over competing technologies with a specific focus on its application to small-to-medium-scale decentralized plants for densification of raw biomass. Despite the inherent positive features of fluidized bed converters, particle heating and time–temperature history, biomass and volatile/gas residence times, gas and solid phases contacting, mixing, and flow pattern need to be carefully controlled to drive conversion along the prescribed chemical pathway.[15] A specific concern regards the course of secondary reactions between depolymerization products and char, whose progress, possibly enhanced by prolonged residence times and uncontrolled backmixing, may alter the quantity/quality of the produced bio-oil. Char, one of the main intermediate products, has been found to aid secondary reactions that degrade primary tars, leading to the formation of lower molecular weight volatiles. The physicochemical characterization of pyrolysis chars has shown that this material has cavities, which may contain active sites (oxygenated functionalities from original biomass matrix degradation) as well as inherent metallic minerals, which may aid secondary reactions.[16] The influence of in-situ (nascent) char on primary volatiles at moderate conditions is of great interest to the pyrolysis process, as greater control of quality may be achieved by controlling the extent of secondary reactions that occur.[17]

There are two possible routes for secondary reactions, the first one considers the catalytic effect of the nascent solid phase (char) heterogeneously influencing primary tar reactions, whereas the second route considers the reactions that occur in the gaseous phase surroundings.[17,18] Heterogeneous reactions can proceed when produced vapours leave the reacting biomass particle, vapours encounter other particles (char, ash, and catalysts) or when vapours are in contact with the (hot) reactor material.[18] Depending on the reactor type, operating conditions, and the size of biomass particles, the extent of heterogeneous secondary reactions between char and primary volatiles may be controlled. Li et al.[19] provide evidence of secondary interaction of primary products of lignin pyrolysis in a fluidized bed converter upon substitution of sand with lignin char as the bed material.

Within fluidized bed operations, a steady char holdup establishes in the bed, regulated by the balance that occurs as fresh biomass is continuously fed while some of the char is subject to elutriation,[18,20] possibly enhanced by attrition.[15,21] Continuous bed drain and regeneration, with the removal of carbon-containing components, may be accomplished to control biomass and char inventories. Char holdup in the bubbling fluidized bed reactor needs to be carefully controlled in order to maintain char freshness if volatile–char interactions are to be carefully controlled,[22] with studies showing that much fresher nascent chars contain oxygen functionalities that may aid in the catalytic activity for low ash biomass feedstocks.

Inevitably, the interactions between volatiles and char are a feature of all biomass pyrolysis reactors as long as more than one feedstock particle is being pyrolyzed. The bulk of the studies on the volatile–char interactions has focused on the influence of alkali and alkaline earth metallic (AAEM) species that are inherently part of the nascent char matrix, as they have been found to exert a much more pronounced effect on the heterogeneous secondary reactions. Reactive—oxygen-containing—functional groups of chars are the key to heterogeneous secondary reactions of low ash-containing materials where the influence of AAEM is minimized.[23] The catalytic nature of nascent chars for pyrolysis heterogeneous secondary reactions has not been sufficiently understood. However, it is believed to play a major role in the reforming of volatiles to form condensable tars. The reaction between nascent char and the

radicals generated during biomass pyrolysis forms the essence of the volatile–char interactions, resulting in the formation of secondary products that are more stable than the primary intermediates. At lower temperatures (500–600°C), less thermally stable nascent tars (such as saccharides, furans, and guaiacols) are prone to char catalytic reactions, while the more thermally stable tars such as phenols and naphthalenes require much higher temperatures (>600°C) for char catalyzed reactions.[23,24]

Volatile–char interactions form the basis of secondary heterogenous reactions that occur during thermochemical devolatilization of biomass.[25] The concentration of AAEM species within the nascent char alters the reactivity of this transient solid intermediate in studies by Du et al.,[26] showing that the reactivity increased two folds in the presences of AAEM species dispersed within the char matrix. In the study by Zhu et al.,[25] secondary pyrolysis reaction, which resulted in the formation of low molecular weight derivatives such as molecular acids, occurred as a result of volatile–char interactions. The presence of potassium in the char also increased the rate of demethoxylation and demethylation of guaiacyl-containing structures leading to the formation of phenols as well as an increased release of CH_4 gas.

Mathematical modelling of biomass pyrolysis in fluidized bed converters has been extensively addressed in the literature.[27–32] It is remarkable, however, that heterogeneous volatile–char secondary reactions have been most often overlooked in reactor modelling, as well as in the setup of pyrolyzer design and operation criteria. Kersten and coworkers,[32,33] upon surveying the relevant literature on the subject, noted that, especially at low temperatures, the contact with char may be more effective on secondary cracking reactions than the actual vapour residence time. They recommend that the char hold-up of the pyrolysis reactor as well as the presence of entrained char in the hot parts of the reactor and the exhaust should be taken into account in reactor modelling and design. The lack of consideration of this aspect may affect the performance of the pyrolyzer as well as the reproducibility of results.

In the present study, careful assessment of fluidized bed fast pyrolysis of biomass is undertaken, based on a simplified compartmental model of a shallow fluidized bed converter with external regeneration of the bed material. The remarkable feature of the model is consideration of heterogeneous volatile–char secondary reactions and a comprehensive representation of the fate of biomass and char, including elutriation, attrition, and bed drain/regeneration for the evaluation of biomass and char loading in the bed. A semi-lumped reaction network, widely adopted in the literature to model biomass primary and homogeneous secondary reactions, has been used in the modelling, complemented by a heterogeneous volatile–char secondary reaction step, whose rate has been modelled by borrowing a kinetic expression for volatile–char interaction in fluidized bed gasifiers. Results of computations provide the basis for the assessment of the role of heterogeneous secondary reactions and for the development of criteria for the optimal design of gas and solids flow patterns and proper management of biomass and char inventories in fluidized beds.

2 | THE FLUIDIZED BED BIOMASS PYROLYZER

Figure 1 reports the scheme of the fluidized bed pyrolyzer that has been assumed as a reference in the model setup. The basic design of the reactor is a shallow bubbling fluidized bed with overbed feeding of the biomass particles. The particle size distribution of the inert bed material is chosen so as to rule out elutriation under typical operating conditions, whereas char elutriation and attrition may take place.

The small aspect ratio of the shallow dense bed and the excess of gas superficial velocity over incipient fluidization are responsible for a considerable fraction of the bed solids hold-up being located in the splashing region of the bed. The prevailing multiphase flow pattern is ejection/fall-back of bed particles promoted by bubbles and spouts bursting at the dense bed surface.[34,35] The combined effects of overbed particle feeding, of biomass particle self-segregation during volatile release[15,36,37] and of extensive particle entrainment and recirculation in the splash zone[38,39] are such that biomass and char particles can be considered well stirred in the splash zone.
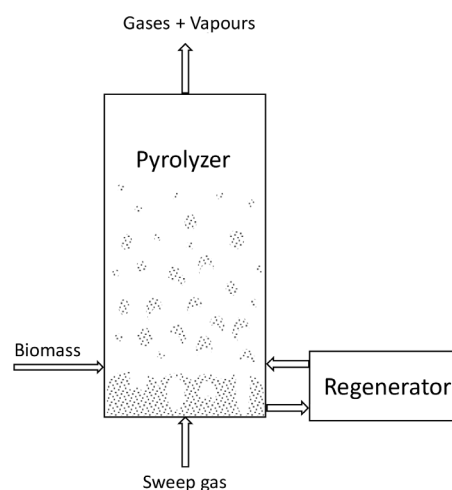

FIGURE 1 Outline of the fluidized bed pyrolyzer

Accordingly, the gas phase is treated as a pseudo-homogeneous phase rather than a bubbly flow, and interphase mass transfer is ignored. Altogether, the reference configuration of the fluidized bed has been chosen so as to accomplish the key functions required for effective control of biomass fast pyrolysis: reliable and manageable feeding of the raw biomass, rapid heating of fuel particles in/above the bottom bed, promoted by 'blanketing' of hot bed solids, efficient mixing, and intimate contact between biomass and char particles and bed material in the splash zone. The confinement of the freeboard height to the splash zone ensures short gas residence time and short contact time between char and pyrolysis vapours, with the target of preventing the course of secondary homogeneous and heterogeneous reactions.

Char accumulation inside the fluidized bed may be controlled by continuously draining bed solids from the bottom of the fluidized bed. The drain stream is further processed in a regenerator where bed material is recovered and recycled to the fluidized bed reactor. Biomass and char are removed from the inert bed material in the regenerator by either combustion or physical separation, depending on the intended further exploitation of the char.

3 | MATHEMATICAL MODEL

The pyrolytic converter is modelled by the means of a 1-D compartmental model, reported in Figure 2, based on a simplified formulation of material balances on lumped components involved in the pyrolytic process. The key features of the model are hereby summarized.
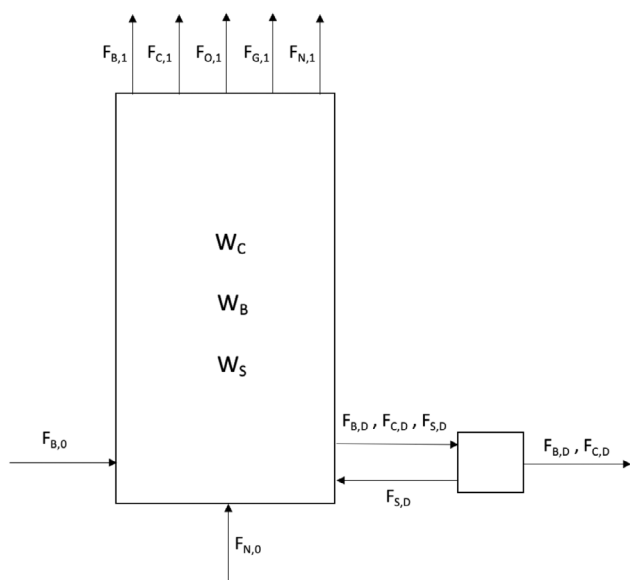

FIGURE 2 Compartmental model of the fluidized bed pyrolyzer

3.1 | Reaction network and kinetics

Figure 3 shows the simplified reaction scheme, similar to that suggested by Shafizadeh and Chin.[40] Table 1 reports the kinetic expressions and parameters used in the model. The scheme considers the classical lumped species: gas (G), oil (O) and char (C) generated by primary pyrolysis of biomass (B). Secondary reactions (4) and (5) account for homogeneous cracking/rearrangement, condensation, and aromatization of oil to gas and/or char. Reaction (6) represents the bundle of secondary heterogeneous reactions between vapours (O) and char in a lumped form. The kinetics of primary reactions is modelled according to expressions proposed by Di Blasi and Branca.[41] The kinetics of secondary homogeneous reactions (4) and (5) are modelled by expressions proposed by Liden et al.[42] and Di Blasi.[43] Due to the lack of specific kinetic data in the literature concerning in situ removal of tars during biomass pyrolysis, information has been searched for in the neighbouring area of tar removal/decomposition by chars and carbons.[45–47] In particular, the kinetics of the heterogenous secondary reaction (6) has been modelled using the expression proposed by Fuentes-Cano et al.[44] for tar decomposition over char, obtained by investigation of conversion of toluene as a surrogate model tar compound over a packed bed of biomass char.

3.2 | Model assumptions

The model is based on the following assumptions:

- The reactor operates under steady-state conditions at atmospheric pressure.
- The shallow bed and the splash zone are treated as a single compartment for the purpose of setting up material balances on bed solids and gas phase.
- Solids are well stirred. An average bed voidage has been assumed in the computations, based on the static bed solids height H_{sb} treated as an input parameter.
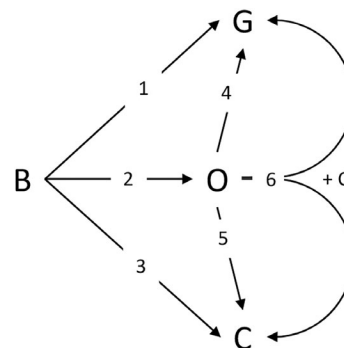

FIGURE 3 The reaction network

TABLE 1 Kinetic parameters of primary and secondary reactions

Reaction	Kinetics $(kg \cdot m^{-3} \cdot s^{-1})$	Pre-exponential factor, $k_{0,i}$	Activation energy, $E_{a,i}$ $(kJ \cdot mol^{-1})$	Ref.
$B \xrightarrow{1} \alpha_1 G$	$r_1 = k_1 C_B$	$4.4 \cdot 10^9$ (s^{-1})	153	Di Blasi and Branca[41]
$B \xrightarrow{2} \beta_2 O$	$r_2 = k_2 C_B$	$1.1 \cdot 10^{10}$ (s^{-1})	148	Di Blasi and Branca[41]
$B \xrightarrow{3} \gamma_3 C$	$r_3 = k_3 C_B$	$3.3 \cdot 10^6$ (s^{-1})	112	Di Blasi and Branca[41]
$O \xrightarrow{4} \alpha_4 G$	$r_4 = k_4 \rho \omega_O$	$4.3 \cdot 10^6$ (s^{-1})	108	Liden et al.[42]
$O \xrightarrow{5} \gamma_5 C$	$r_5 = k_5 \rho \omega_O$	$1 \cdot 10^5$ (s^{-1})	108	Di Blasi[43]
$O \xrightarrow{6, +C} \alpha_6 G + \gamma_6 C$	$r_6 = k_6 C_C \rho \omega_O$	86.1 $(m^3 kg^{-1} s^{-1})$	75	Fuentes-Cano et al.[44]

TABLE 2 Model equations

	Balance equations
Biomass	$F_{B,0} - W_B(k_1 + k_2 + k_3) - F_{B,E} - F_{B,D} = 0$
	$F_{B,E} = F_{el,B} + F_{a,B}$
Char	$W_B \gamma_3 k_3 + R_{5,C} + R_{6,C} - F_{C,E} - F_{C,D} = 0$
	$R_{5,C} = \gamma_5 S \int_0^{L_E} k_5 \varepsilon \rho \omega_O dz$
	$R_{6,C} = \gamma_6 \frac{W_C}{L_E} \int_0^{L_E} k_6 \rho \omega_O dz$
	$F_{C,E} = F_{el,C} + F_{a,C}$
Oil	$\frac{d(Q\rho\omega_O)}{dz} = S\overline{D}\frac{d}{dz}\left(\rho \frac{d\omega_O}{dz}\right) + \beta_2 k_2 \frac{W_B}{L_E} - \varepsilon S k_4 \rho \omega_O - \varepsilon S k_5 \rho \omega_O - k_6 \rho \omega_O \frac{W_C}{L_E}$
Gas	$\frac{d(Q\rho\omega_G)}{dz} = S\overline{D}\frac{d}{dz}\left(\rho \frac{d\omega_G}{dz}\right) + \alpha_1 k_1 \frac{W_B}{L_E} + \varepsilon S \alpha_4 k_4 \rho \omega_O + \alpha_6 k_6 \rho \omega_O \frac{W_C}{L_E}$
Sweep gas	$\frac{d}{dz}[Q\rho(1 - \omega_O - \omega_G)] = 0$
	Constitutive equations
Elutriation rate[a]	$F_{el,i} = k_{el,i} W_i$
Elutriation rate constant[a]	$k_{el,i} = K_{i,\infty}^* \frac{S}{\sum_i W_i}$ $\qquad$ $\frac{K_{i,\infty}^*}{\rho_G U} = 23.7 \cdot \exp\left(-5.4 \frac{U_{t,i}}{U}\right)$
Attrition rate[a]	$F_{a,i} = k_{a,i} \frac{U - U_{mf}}{d_{p,i}} W_i$
Gas-phase density[b]	$\rho = \frac{P}{RT} \frac{1}{\sum_i \frac{\omega_i}{M_i}}$
Average velocity	$U = \frac{\frac{1}{L_E}\int_0^{L_E} Q dz}{S}$
Drainage space–time[c]	$\tau_D = \frac{W_i}{F_{i,D}} = \frac{\sum_i W_i}{\sum_i F_{i,D}}$
Boundary conditions	$z = 0 \rightarrow Q = \frac{RT}{P}\frac{F_{N,0}}{PM_N}; 0 = Q\rho\omega_O - S\overline{D}\rho\frac{d\omega_O}{dz}; 0 = Q\rho\omega_G - S\overline{D}\rho\frac{d\omega_G}{dz}$
	$z = L_E \rightarrow \frac{d\rho\omega_O}{dz} = \frac{d\rho\omega_G}{dz} = 0$

[a] $i = B, C$.
[b] $i = O, G, N$.
[c] $i = B, C, S$.

- Temperature is uniform in the reactor and thermal equilibrium among phases holds.
- All compounds in the gas phase behave as ideal gases.
- The gas phase flow pattern is described by the axial dispersion model with variable mixture density, following the approach described by Douglas and Bischoff.[48]

The axial dispersion coefficient is assumed constant and calculated considering the axially averaged value of the gas velocity.

- Biomass particles are small enough (<1 mm in diameter) for the effect of particle shrinkage and intraparticle thermal nonuniformities to be negligible. Accordingly,

pyrolysis of biomass is described by the progressive conversion model, in which a constant biomass particle size is assumed while its density decreases due to increasing porosity during the course of the reaction.[31]

- The bed material is inert and exerts no catalytic activity on whatever reaction it supports.
- Attrited fines are instantaneously elutriated from the reactor.
- Reaction of steam with char is neglected.

3.3 | Model equations

A scheme of the compartmental model of the pyrolyzer with the inlet and outlet streams is reported in Figure 2. Model equations are reported in Table 2. Mass balances are expressed for the raw biomass B, the pyrolysis products (char, C; oil, O; and gas, G) and for the sweep gas (assumed with the properties of nitrogen).

Elutriation of biomass and char particles is taken into account, assuming the expression for the elutriation flux constant $K_{i,\infty}^*$ proposed by Geldart et al. and Tasirin and Geldart.[49,50] Attrition by abrasion is assumed to be negligible for biomass particles ($F_{a,B} = 0$). Attrition of char particles is modelled, assuming the constitutive equation and the attrition constant $k_{a,C}$ proposed by Scala et al.[21] Accordingly, the attrition rate is directly proportional to char inventory and to the excess gas superficial velocity with respect to the incipient fluidization velocity and is inversely proportional to char particle size. The correlations for the minimum fluidization velocity U_{mf} of the bed material and for the terminal velocity $U_{t,i}$ of each solid component are taken from Wen and Yu[51] and Haider and Levenspiel,[52] respectively. The ideal gas equation of state is used to calculate the mixture density, hence the volumetric flow rate and the gas superficial velocity U averaged along the axial coordinate. A space–time τ_D is introduced as the ratio of the solids inventory and the solids drain rate. The assumption that solids are well stirred implies that the concentration of each solid component in the bed equals that in the drainage, hence τ_D is the same for all the solids components.

The model has been further simplified by assuming constant gas flow rate and bed voidage along the reactor coordinate z. In order to assess the role of gas backmixing, computations have been performed with reference to the two limiting cases, as regards the flow pattern of the gas phase:

Case I) $D = 0$ plug flow of the gas phase (plug flow reactor, PFR)

Case II) $D \to \infty$ perfect mixing of the gas phase (continuous stirred tank reactor, CSTR)

With the above reported assumptions, the differential equation expressing the material balance on oil may be integrated analytically, yielding:

Case I) PFR

$$C_O(z) = \frac{\chi}{\phi}[1 - \exp(-\phi z)] \tag{1}$$

$$C_{O,E} = \frac{\chi}{\phi}[1 - \exp(-\phi L_E)] \tag{2}$$

$$C_G(z) = (\xi + \psi)z - \frac{\psi}{\phi}[1 - \exp(-\phi z)] \tag{3}$$

$$C_{G,E} = (\xi + \psi)L_E - \frac{\psi}{\phi}[1 - \exp(-\phi L_E)] \tag{4}$$

where $\phi = \frac{1}{U}\left(\varepsilon k_4 + \varepsilon k_5 + k_6 \frac{W_C}{V}\right)$; $\chi = \frac{1}{U}\beta_2 k_2 \frac{W_B}{V}$; $\psi = \frac{1}{U}\left(\varepsilon \alpha_4 k_4 + \alpha_6 k_6 \frac{W_C}{V}\right)\frac{\chi}{\phi}$ and $\xi = \frac{1}{U}\alpha_1 k_1 \frac{W_B}{V}$.

Case II) CSTR

$$C_{O,E} = \frac{\beta_2 k_2 W_B}{SU + \varepsilon V k_4 + \varepsilon V k_5 + k_6 W_C} \tag{5}$$

$$C_{G,E} = \frac{\alpha_1 k_1 W_B + (\varepsilon V \alpha_4 k_4 + \alpha_6 k_6 W_C)C_{O,E}}{SU} \tag{6}$$

In either case, the material balance on oil is coupled with biomass and char material balances by the following equations, respectively:

$$W_B = \frac{F_{B,0}}{k_1 + k_2 + k_3 + k_{el,B} + \frac{1}{\tau_D}} \tag{7}$$

$$W_C = \frac{k_3 \gamma_3 W_B + k_5 \gamma_5 \varepsilon V \cdot \langle C_O \rangle}{k_{el,C} + \frac{1}{\tau_D} - k_6 \gamma_6 \cdot \langle C_O \rangle + k_{a,C}\frac{U - U_{mf}}{d_p}W_C} \tag{8}$$

where

$$\langle C_O \rangle = \begin{cases} \frac{1}{L_E}\int_0^{L_E} C_O(z)dz \text{ for case I} \\ C_{O,E} \text{ for case II} \end{cases} \tag{9}$$

The solution of the model equations requires an iterative trial-and-error procedure on the biomass and char inventories, whose convergence is straightforward. Values for the attrition constant, properties of the fluid and the solid components, and other input parameters for the base-case model computations are reported in Table 3. The stoichiometric coefficients in Table 1 were all set equal to 1, with the exception of α_6 and γ_6. There is currently a lack of information on plausible values of these coefficients. Within the present study values, they were set at $\alpha_6 = 0.2$ and $\gamma_6 = 0.8$ on account of trends suggested by Fuentes-Cano et al.,[44] according to which carbon deposition dominates tar conversion at moderate temperatures. Better characterization of mechanisms and rates of secondary reactions between pyrolysis vapours and bio-char at conditions relevant to biomass pyrolysis is clearly a research priority.

The biomass feed rate and the sweep gas flow rate per unit cross-sectional area of the pyrolyzer were set at values typical of the operating conditions of bubbling fluidized bed pyrolyzers reported in the literature.

4 | RESULTS AND DISCUSSION

Oil and gas yields are reported in Figure 4 as a function of the drainage space–time τ_D for the two limiting cases

referred to by the gas phase flow pattern: plug flow, PFR; perfect mixing, CSTR. In the PFR limiting case, the oil yield η_O first increases to a maximum value of around 0.59, and then it slowly decreases for increasing values of τ_D. The decrease in η_O for large values of τ_D reflects the increased value of bed char loading, hence, larger contribution of oil–char interaction to heterogeneous secondary conversion of bio-oil. For the CSTR limiting case, a similar trend of η_O is obtained, with a maximum value around 0.49. For very small τ_D, the fairly limited values of oil and gas yields are the consequence of extensive drainage of unconverted raw biomass from the bed. Altogether, backmixing turns out to be detrimental to the pyrolyzer performance, a feature that is fully consistent
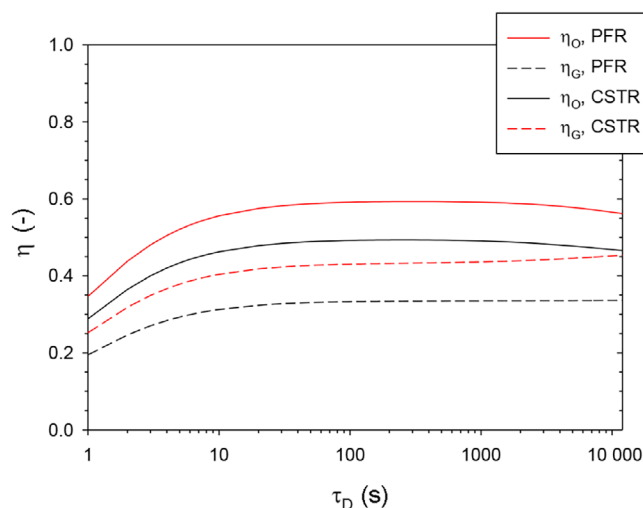

FIGURE 4 Oil and gas yields as a function of drainage space–time. Comparison of results for plug flow reactor (PFR) and continuous stirred tank reactor (CSTR) limiting cases
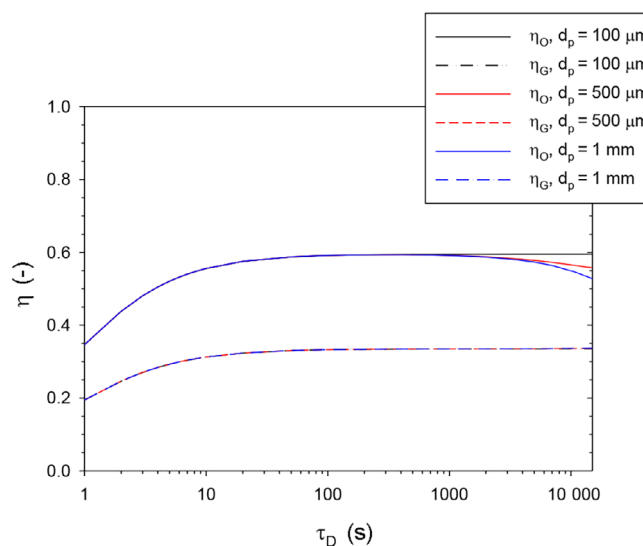
TABLE 3 Input parameters and physical properties of the solid phases

Parameter	Value
P (atm)	1
T (K)	773
L_E (m)	1
H_{sb} (m)	0.35
S (m^2)[a]	1
U (m · s^{-1})	0.3
d_p (μm)	500
d_S (μm)	500
$U_{t,B}$ (m · s^{-1})	2.2
$U_{t,C}$ (m · s^{-1})	0.81
$k_{a,C}$ (−)	$3 \cdot 10^{-7}$
$F_{B,0}$ (kg · s^{-1})	0.1
$F_{N,0}$ (kg · s^{-1})	0.13
Q (Nm^3 · s^{-1})	0.1
ρ_B (kg · m^{-3})	1000
ρ_C (kg · m^{-3})	300
ρ_S (kg · m^{-3})	2600

[a]1 · 1 m square cross-section.

FIGURE 5 Oil and gas yields as a function of drainage space–time for different values of biomass particle size
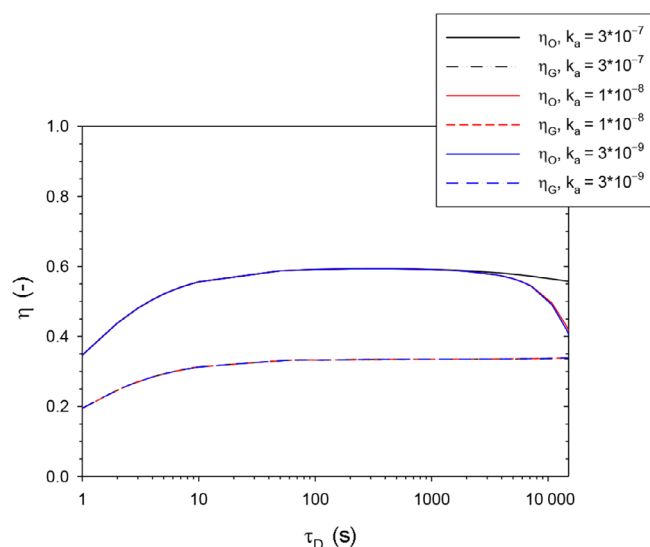
FIGURE 6 Oil and gas yields as a function of drainage space–time for different values of the char abrasion constant

FIGURE 7 Oil and gas yields as a function of drainage space–time for different values of the gas superficial velocity

with fundamental chemical reaction engineering principles when one considers that the desired product O is an intermediate product of serial primary and secondary reactions. The gap $\Delta\eta_O$ in the oil yields in the two cases is within 20% when τ_D is set in the optimal range of 100–1000 s. Of course, a converter featuring non-ideal behaviour, that is, a finite value of the axial dispersion coefficient D, would display an intermediate yield between those of the PFR and CSTR limiting cases.

The effect of biomass and char particle size on oil and gas yields is shown in Figure 5 as a function of τ_D. For $d_p = 100\,\mu m$, η_O and η_G increase with τ_D to reach a constant value around 0.6 and 0.33, respectively. For $d_p = 500\,\mu m$ and 1 mm, η_O first increases to a maximum value and then, for very large τ_D, it decreases. Deeper inspection of the concurrent paths responsible for char leaving the bed indicated that attrition by abrasion dominates over elutriation and is the dominant process balancing char accumulation for large drainage space–times, say larger than 500 s. For small values of τ_D, instead, abrasion is overcome by the char drainage. The correspondingly smaller value of char loading in the bed is consistent with a declining role of heterogeneous secondary reactions. As a matter of fact η_O^{max} assumes nearly the same value for all the particle sizes investigated. Instead, for large values of τ_D, the oil yield decreases with the increasing particle size. This is due to a smaller abrasion rate as the particle size is increased, resulting in a larger amount of char accumulating in the bed. Accordingly, the role of secondary heterogeneous reactions is emphasized, and the oil yield decreases. Gas yield is only moderately affected at large drainage space–times. This is most likely the consequence of the stoichiometry ($\alpha_6 = 0.2$; $\gamma_6 = 0.8$)
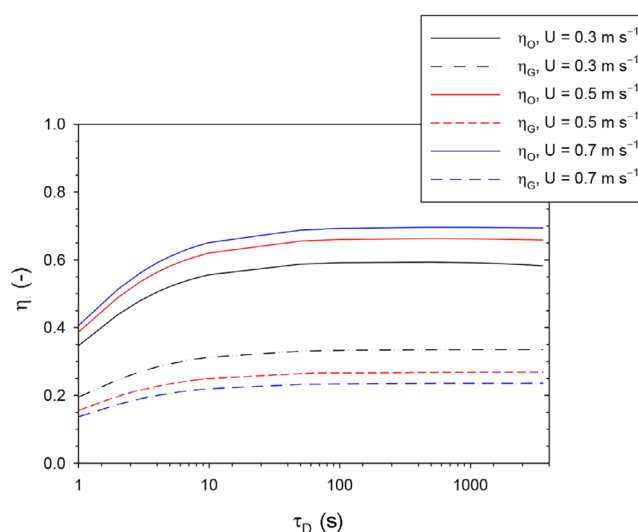
assumed in the computations, which is consistent with a predominant yield to C, rather than G, as oil undergoes heterogeneous secondary conversion along reaction (6).

The sensitivity of oil and gas yields to the value of the char abrasion constant may be appreciated in Figure 6, as a function of τ_D. Computations have been performed, assuming typical values of $k_{a,C}$ reported in the literature for three kinds of biomass, wood chips ($k_{a,C} = 3 \cdot 10^{-7}$), pine seed shells ($k_{a,C} = 1 \cdot 10^{-8}$), and olive husks ($k_{a,C} = 3 \cdot 10^{-9}$).[21] Oil yields reach the maximum value for τ_D around 200 s for all the values of $k_{a,C}$ considered. Thereby, η_O remains fairly constant and slightly decreases for very large values of the drain space–time. In fact, the effect of the abrasion constant on the oil yield starts to be evident for τ_D larger than 10^3 s, with η_O decreasing for smaller values of the abrasion constant. This result highlights the role of attrition by abrasion on char loading in the bed and, accordingly, on the effect of secondary heterogeneous reactions on product yields. For τ_D smaller than about 1000 s, attrition by abrasion does not significantly influence the yields, as for the selected values of $k_{a,C}$, the change in char loading due to abrasion is overcome by bed drain. On the other hand, gas yield increases with τ_D to remain nearly constant. Then, for τ_D larger than 1000 s, gas yield is nearly independent from the value of $k_{a,C}$, as for very high τ_D, secondary reactions have a very slight impact on the gas yield.

The effect of the gas superficial velocity on oil and gas yields is reported in Figure 7 as a function of τ_D. It can be seen that both oil and gas yields first increase with τ_D and then approach a nearly constant value for τ_D larger than about 100 s for all the values of U considered in the computations.

The favourable effect of increasing U on oil yield η_O can be explained in the light of the combined effects of the smaller residence time of pyrolysis vapours and of enhanced char attrition, both hampering secondary reactions. It must be recalled that elutriation of biomass might be enhanced by a further increase in gas superficial velocity and might jeopardize product yields. However, it is fairly limited in the range of operating conditions considered in the computations.

5 | CONCLUSIONS

The results of model computations based on a compartmental 1-D model of a fluidized bed fast pyrolyzer have been directed to shed light on some key phenomena affecting product yield and selectivity. Unlike most previously published models, in this study, special attention has been paid to the assessment of the possible role of secondary heterogeneous reactions between primary pyrolysis vapours and the bio-char accumulated in the bed. Results support the view that char-vapour secondary reactions cannot be disregarded and underline the importance of careful management of char inventory in the converter. Char loading in the bed depends on the combination of char particle elutriation, attrition, and bed drain/regeneration. Results demonstrate the criticality of thorough experimental characterization and control of biomass char attrition as the dominant modes to balance char accumulation in the bed when bed drain is not accomplished. Results give also clear indication of criteria for optimal management of bed drain/regeneration and highlight the detrimental role of gas-phase backmixing. Better characterization of mechanisms and rate of secondary reactions between pyrolysis vapours and biochar at conditions relevant to biomass pyrolysis represents no doubt a research priority.

Altogether, despite the simplifying assumptions on which the present 'learning' model is based, results of computations are helpful in shedding light on the sensitivity of bio-oil yield on selected process variables and specifically on char inventory in the bed and on the associated course of secondary heterogeneous reactions of primary pyrolysis vapours. The model provides useful support for the setup criteria for optimal design and operation of the pyrolyzer and lays the path for more comprehensive models characterized by full predictive ability.

NOMENCLATURE
Symbols
D	axial dispersion coefficient ($m^2 \cdot s^{-1}$)
d_p	biomass/char particle diameter (m)
d_S	bed inert particle diameter (m)
E_a	activation energy ($kJ \cdot mol^{-1}$)
F	mass flow rate ($kg \cdot s^{-1}$)
H_{sb}	static bed height (m)
k	kinetic rate constant
$k_{0,j}$	pre-exponential factor of the jth reaction (s^{-1})
k_{el}	elutriation rate constant (s^{-1})
$K^*_{i,\infty}$	elutriation flux constant for the ith species ($kg \cdot m^{-2} \cdot s^{-1}$)
L_E	length of the converter (m)
M	molecular weight ($kg \cdot kmol^{-1}$)
P	pressure (atm)
Q	volumetric gas flow rate ($m^3 \cdot s^{-1}$)
r	reaction rate ($kg \cdot m^{-3} \cdot s^{-1}$)
R	universal ideal gas constant ($J \cdot mol^{-1} \cdot K^{-1}$)
$R_{j,i}$	axially averaged reaction rate ($kg \cdot s^{-1}$)
S	bed cross-sectional area (m^2)
T	temperature (K)
U	average gas velocity ($m \cdot s^{-1}$)
V	reactor volume (m^3)
W	mass (kg)
z	axial coordinate (m)

Greek letters
α	stoichiometric coefficient of gas phase ($-$)
β	stoichiometric coefficient of biomass phase ($-$)
γ	stoichiometric coefficient of char phase ($-$)
ε	average voidage ($-$)
η	fractional yield ($-$)
ρ	density ($kg \cdot m^{-3}$)
τ	space time (s)
ω	mass fraction ($-$)

Subscripts
0	relative to the inlet
a	relative to attrition by abrasion
B	biomass
C	char
D	drainage
E	exit
G	gas species number
i,j	reaction number
mf	minimum fluidization
N	nitrogen, sweep gas
O	oil
S	sand
t	terminal

review and editing. **Elvis Tinashe Ganda:** Conceptualization; data curation; investigation; methodology; writing – original draft; writing – review and editing. **Piero Salatino:** Conceptualization; investigation; methodology; supervision; writing – original draft; writing – review and editing.

PEER REVIEW
The peer review history for this article is available at https://publons.com/publon/10.1002/cjce.24616.

DATA AVAILABILITY STATEMENT
I hereby declare that the data that support the findings of this study are available from the corresponding author upon reasonable request.

ORCID
Piero Salatino https://orcid.org/0000-0002-0002-1691

REFERENCES
[1] S. S. Hassan, G. A. Williams, A. K. Jaiswal, *Trends Biotechnol.* **2019**, *37*, 231.
[2] A. V. Bridgwater, in *Pyrolysis of Solid Biomass: Basics, Processes, and Products - Encyclopedia of Sustainability Science and Technology* (Ed: R. A. Meyers), Springer, New York **2017**, p. 1.
[3] K. Kang, N. B. Klinghoffer, I. ElGhamrawy, F. Berruti, *Renewable Sustainable Energy Rev.* **2021**, *149*, 111372.
[4] G. W. Huber, S. Iborra, A. Corma, *Chem. Rev.* **2006**, *106*, 4044.
[5] S. Wang, G. Dai, H. Yang, Z. Luo, *Prog. Energy Combust. Sci.* **2017**, *62*, 33.
[6] K. N. Yogalakshmi, T. Poornima Devi, P. Sivashanmugam, S. Kavitha, R. Yukesh Kannah, S. Varjani, S. AdishKumar, G. Kumar, J. Rajesh Banu, *Chemosphere* **2022**, *286*, 131824.
[7] S. Czernik, A. V. Bridgwater, *Energy Fuels* **2004**, *18*, 590.
[8] M. Olazar, R. Aguado, J. Bilbao, A. Barona, *AIChE J.* **2000**, *46*, 1025.
[9] T. R. Carlson, Y.-T. Cheng, J. Jae, G. W. Huber, *Energy Environ. Sci.* **2011**, *4*, 145.
[10] V. Paasikallio, F. Agblevor, A. Oasmaa, J. Lehto, J. Lehtonen, *Energy Fuels* **2013**, *27*, 7587.
[11] G. Yildiz, F. Ronsse, R. van Duren, W. Prins, *Renewable Sustainable Energy Rev.* **2016**, *57*, 1596.
[12] H. Hernando, G. Gómez-Pozuelo, J. A. Botas, D. P. Serrano, *J. Anal. Appl. Pyrolysis* **2021**, *154*, 105019.
[13] L. Luque, R. Westerhof, G. Van Rossum, S. Oudenhoven, S. Kersten, F. Berruti, L. Rehmann, *Bioresour. Technol.* **2014**, *161*, 20.
[14] Z. Wang, K. G. Burra, T. Lei, A. K. Gupta, *Prog. Energy Combust. Sci.* **2021**, *84*, 100899.
[15] P. Salatino, R. Solimene, *Powder Technol.* **2017**, *316*, 29.
[16] C. A. Koufopanos, N. Papayannakos, G. Maschio, A. Lucchesi, *Can. J. Chem. Eng.* **1991**, *69*, 907.
[17] M. L. Boroson, J. B. Howard, J. P. Longwell, W. A. Peters, *Energy Fuels* **1989**, *3*, 735.
[18] E. Hoekstra, R. J. M. Westerhof, W. Brilman, W. P. M. Van Swaaij, S. R. A. Kersten, K. J. A. Hogendoorn, M. Windt, *AIChE J.* **2012**, *58*, 2830.
[19] D. Li, C. Briens, F. Berruti, *Bioresour. Technol.* **2015**, *189*, 7.
[20] C.-Z. Li, *Fuel* **2013**, *112*, 609.
[21] F. Scala, R. Chirone, P. Salatino, *Energy Fuels* **2006**, *20*, 91.
[22] D. M. Keown, J. Hayashi, C.-Z. Li, *Fuel* **2008**, *87*, 1187.
[23] Y. Huang, S. Liu, M. A. Akhtar, B. Li, J. Zhou, S. Zhang, H. Zhang, *Bioresour. Technol.* **2020**, *316*, 123938.
[24] Q. Sun, S. Yu, F. Wang, J. Wang, *Fuel* **2011**, *90*, 1041.
[25] H. Zhu, B. Yi, H. Hu, Q. Fan, H. Wang, H. Yao, *Energy* **2021**, *214*, 119065.
[26] C. Du, L. Liu, P. Qiu, *RSC Adv.* **2017**, *7*, 10397.
[27] A. Blanco, F. Chejne, *J. Anal. Appl. Pyrolysis* **2016**, *118*, 105.
[28] J. F. Peters, S. W. Banks, A. V. Bridgwater, J. Dufour, *Appl. Energy* **2017**, *188*, 595.
[29] G. Lopez, J. Alvarez, M. Amutio, B. Hooshdaran, M. Cortazar, M. Haghshenasfard, S. H. Hosseini, M. Olazar, *Chem. Eng. J.* **2019**, *373*, 677.
[30] P. Kaushal, J. Abedi, *J. Ind. Eng. Chem.* **2010**, *16*, 748.
[31] B. Hejazi, J. R. Grace, X. Bi, A. Mahecha-Botero, *J. Anal. Appl. Pyrolysis* **2016**, *121*, 213.
[32] S. R. A. Kersten, X. Wang, W. Prins, W. P. M. van Swaaij, *Ind. Eng. Chem. Res.* **2005**, *44*, 8773.
[33] X. Wang, S. R. A. Kersten, W. Prins, W. P. M. van Swaaij, *Ind. Eng. Chem. Res.* **2005**, *44*, 8786.
[34] L. M. Garcia-Gutierrez, A. Soria-Verdugo, C. Marugán-Cruz, U. Ruiz-Rivas, *Powder Technol.* **2014**, *263*, 112.
[35] J. A. Almendros-Ibáñez, S. Sánchez-Delgado, C. Sobrino, D. Santana, *Chem. Eng. Process.* **2009**, *48*, 734.
[36] G. Bruni, R. Solimene, A. Marzocchella, P. Salatino, J. G. Yates, P. Lettieri, M. Fiorentino, *Powder Technol.* **2002**, *128*, 11.
[37] S. Iannello, P. U. Foscolo, M. Materazzi, *Chem. Eng. J.* **2022**, *431*, 133807.
[38] T. Djerf, D. Pallarès, F. Johnsson, *Fuel Process. Technol.* **2018**, *173*, 112.
[39] A. Köhler, D. Pallarès, F. Johnsson, *Energy Fuels* **2020**, *34*, 3294.
[40] F. Shafizadeh, P. P. S. Chin, in *Wood Technology: Chemical Aspects*, Vol. 43 (Eds: F. Shafizadeh, P. P. S. Chin), ACS Publications, Washington, DC **1977**, p. 57.

[41] C. Di Blasi, C. Branca, *Ind. Eng. Chem. Res.* **2001**, *40*, 5547.

[42] A. G. Liden, F. Berruti, D. S. Scott, *Chem. Eng. Commun.* **1988**, *65*, 207.

[43] C. Di Blasi, *Combust. Sci. Technol.* **1993**, *90*, 315.

[44] D. Fuentes-Cano, A. Gómez-Barea, S. Nilsson, P. Ollero, *Chem. Eng. J.* **2013**, *228*, 1223.

[45] G. Ravenni, Z. Sárossy, J. Ahrenfeldt, U. B. Henriksen, *Renewable Sustainable Energy Rev.* **2018**, *94*, 1044.

[46] Y. Shen, *Renewable Sustainable Energy Rev.* **2015**, *43*, 281.

[47] L. Cheng, Z. Wu, Z. Zhang, C. Guo, N. Ellis, X. Bi, A. Paul Watkinson, J. R. Grace, *Appl. Energy* **2020**, *258*, 114088.

[48] J. M. Douglas, K. B. Bischoff, *Ind. Eng. Chem. Process Des. Dev.* **1964**, *3*, 130.

[49] D. Geldart, J. Cullinan, S. Georghiades, D. Gilvray, D. J. Pope, *Trans. Inst. Chem. Eng.* **1979**, *57*, 269.

[50] S. M. Tasirin, D. Geldart, *Powder Technol.* **1998**, *95*, 240.

[51] C. Y. Wen, Y. H. Yu, *AIChE J.* **1966**, *12*, 610.

[52] A. Haider, O. Levenspiel, *Powder Technol.* **1989**, *58*, 63.